Research Journal of Applied Sciences, Engineering and Technology 7(11): 2286-2297, 2014
DOI:10.19026/rjaset.7.528
ISSN: 2040-7459; e-ISSN: 2040-7467

Submitted: July 15, 2013 Accepted: August 05, 2013 Published: March 20, 2014

Research Article

Comparison and Assessment of a Multiple Optimal Coordinated Design Based on PSS and the STATCOM Device for Damping Power System Oscillations

A.N. Hussain, F. Malek, M.A. Rashid and L. Mohamed
School of Electrical Systems Engineering, University Malaysia Perlis (UniMAP) Pauh, Arau, Perlis, Malaysia

Abstract: The aim of this study is to present a comprehensive comparison and assessment of the damping function improvement for the multiple damping stabilizers using the simultaneously coordinated design based on Power System Stabilizer (PSS) and Static synchronous Compensator (STATCOM). In electrical power system, the STATCOM device is used to support bus voltage by compensating reactive power; it is also capable of enhancing the stability of the power system by the adding a supplementary damping stabilizer to the internal AC or DC voltage control channel of the STATCOM inputs to serve as a Power Oscillation Damping (POD) controller. Simultaneous coordination can be performed in different ways. First, the dual-coordinated design between PSS and STATCOM AC-POD stabilizer or DC-POD stabilizer is used. Then, coordination between the AC and DC STATCOM-based POD stabilizers are arranged in a single STATCOM device without PSS. Second, the coordinated design has been extended to triple multiple stabilizers among PSS, the AC-based POD and the DC-based POD in a Single Machine Infinite Bus (SMIB). The parameters of the multiple stabilizers have been tuned in the coordinated design by using a Chaotic Particle Swarm Optimization (CPSO) algorithm that optimized the given eigenvalue-based objective function. The simulation results show that the dual-coordinated design provide satisfactory damping performance over the individual control responses. Furthermore, the-triple coordinated design has been shown to be more effective in damping oscillations than the dual damping stabilizers.

Keywords: Power system oscillation damping, PSS, STATCOM, triple coordinated design

INTRODUCTION

Modern power systems are complex and frequently exhibit low-frequency, electromechanical oscillations due to inadequate damping caused by adverse operating conditions. Low-Frequency Oscillations (LFO) can severely constrain the operation of a system and can decrease the security level of the power system (Abido, 2005; Mostafa *et al*., 2012).

Over the past few decades, Power System Stabilizers (PSSs) have been used extensively for damping electromechanical oscillations in power systems (Furini *et al*., 2011). The damping effect of a PSS is valid only for small trips around the operating point. When the loading conditions and system parameters change significantly, the synchronism of the system can be lost (Li *et al*., 2009). Therefore, the use of PSSs alone may not provide adequate damping for the oscillations of a large power system (Abdel-Magid and Abido, 2004).

STATCOM devices are present in the power system to provide dynamic shunt compensation to support the bus voltage by injecting or absorbing reactive power; they also are capable of improving the stability of the power system (Babaei *et al*., 2011). The main idea of a functional control for damping power oscillations, referred to as a STATCOM supplementary Power Oscillation Damping controller (POD), could be designed to modulate the bus voltage of the STATCOM in order to improve the damping of system oscillations (Panda and Padhy, 2008).

To improve overall system performance, the technique that is most often used is to arrange multiple damping controllers, but the interaction among them may cause destabilization of the damping of the system's oscillations. In order to overcome the problem of interactions among multiple damping controllers, a coordinated design is required to gain the benefits of multiple stabilizers, thereby enhancing the stability of the system and to reduce any possible negative interactions among the different-stabilizers. One approach for achieving the required performance is to design the coordination of the controllers based on previous knowledge of the system's characteristics so as to

Corresponding Author: A.N. Hussain, School of Electrical Systems Engineering, University Malaysia Perlis (UniMAP) Pauh, Arau, Perlis, Malaysia, Tel.: +6-0196560602

provide optimal constraints on negative interactions (Gibbard *et al*., 2000; Zhang *et al*., 2006).

Hence, the use of optimization techniques must be efficient and quick and it must ensure the security of dynamic system in case critical events occur.

Many artificial intelligence techniques have been used to provide the desired coordinated design and robustness of multiple stabilizers, including the application of artificial neural networks (Nguyen and Gianto, 2008; Segal *et al*., 2004), genetic algorithms (Abdel-Magid and Abido, 2004; Rouco, 2001), fuzzy logic control (Kazemi and Sohrforouzani, 2006; Mukherjee and Ghoshal, 2007), bacterial foraging algorithm (Abd-Elazim and Ali, 2012) and various combinations of these approaches (Talaat *et al*., 2010; Mohagheghi *et al*., 2007).

Recently, the Particle Swarm Optimization (PSO) technique has appeared as a useful tool for engineering global optimization to solve the coordinated design problem of multiple power system stabilizers (Mostafa *et al*., 2012; Du *et al*., 2010; Hemmati *et al*., 2011; Shayeghi *et al*., 2010).

In this study, we present the results of our comprehensive comparison and assessment of the damping function of multiple damping stabilizers using different coordinated designs in order to identify the design that provided the most effective damping performance. The three alternative designs we evaluated are listed below:

- Dual-coordinated design between PSS and STATCOM AC-POD or PSS and STATCOM DC-POD
- Dual-coordinated design between STATCOM AC-POD and STATCOM DC-POD arranged in a single STATCOM device without PSS
- Triple-coordinated design among PSS, STATCOM AC-POD and STATCOM DC-POD

The PSO technique was used for tuning the parameters of the multiple damping stabilizers in the coordinated design based on an eigenvalue objective function. Simulation results for a Single Machine Infinite Bus (SMIB) equipped with STATCOM showed that, for a wide range of operating conditions, the triple-coordinated design had better damping ability for LFO than the dual-coordinated design, which enhanced the stability of the power system significantly.

OPTIMAL COORDINATED DESIGN METHODS FOR THE MULTIPLE DAMPING STABILIZERS

Nonlinear models of the generator and excitation system: In this study, as shown in Fig. 1, we considered SMIB system equipped with a STATCOM installed at a point m in the transmission line. The synchronous generator was equipped with a PSS and it supplied

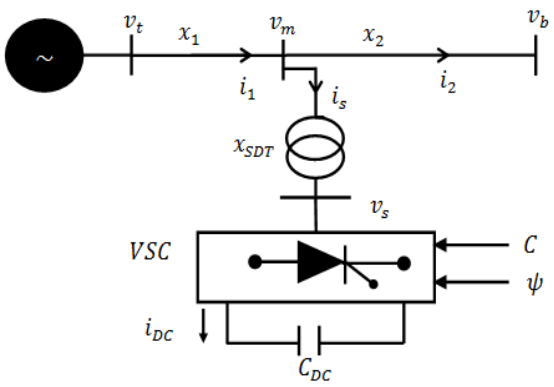

Fig. 1: SMIB power system installer with a STATCOM

power to the infinite bus through a transmission line and a STATCOM.

The generator can be represented by a third-order model comprised of the electromechanical swing equation and the generator internal voltage equation (Yao, 1983).

The swing equation is divided into the following equations:

$$\frac{d\delta}{dt} = \omega_b(\omega - 1) \quad (1)$$

$$\frac{d\omega}{dt} = \frac{1}{M}[P_m - P_e - D(\omega - 1)] \quad (2)$$

$$\frac{d\dot{E}_q}{dt} = \frac{1}{T'_{do}}\left[E_{fd} - E_q\right] \quad (3)$$

where,

ω_b = The synchronous speed

δ and ω = The angle and speed of the rotor respectively

P_m and P_e = The input mechanical and output electrical power of the generator, respectively

M and D = The machine inertia constant and damping coefficient, respectively

E_{fd} = The generator field voltage

T'_{do} = The open-circuit field time constant

The output power of the generator can be expressed in terms of the d-axis and q-axis components of the armature current i and the terminal voltage v_t as:

$$P_e = v_{td}i_d + v_{tq}i_q \quad (4)$$

$$v_t = v_{td} + jv_{tq} \quad (5)$$

$$v_{td} = x_q i_q, v_{tq} = E'_q - \dot{x}_d i_d \quad (6)$$

$$E_q = E'_q + i_d(x_d - \dot{x}_d), i = i_d + i_q \quad (7)$$

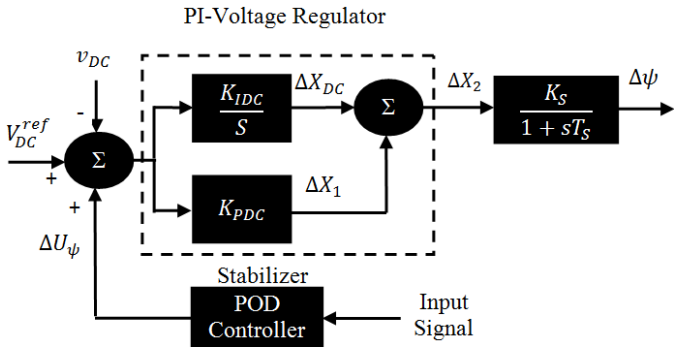

Fig. 2: STACOM dynamic model of DC voltage regulator and POD stabilizer

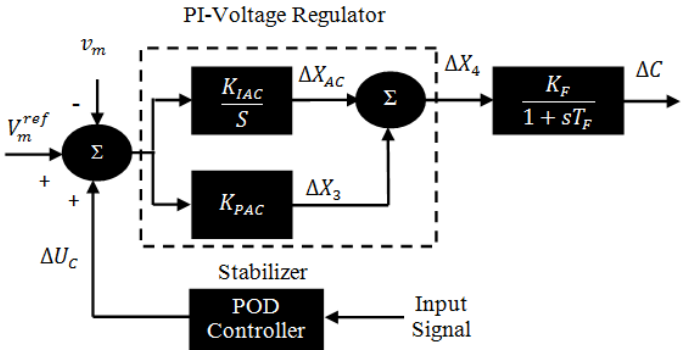

Fig. 3: STACOM dynamic model of AC voltage regulator and POD stabilizer

where,

$\dot{x}_d$ = The d-axis transient reactance
x_q = The q-axis reactance
$E_q^{'}$ = The transient generator internal voltage

The excitation system is represented by a first order model (IEEE type-ST1) (Kamwa *et al*., 2000):

$$\frac{dE_{fd}}{dt} = \frac{1}{T_a}\left[K_a\left(V_{ref} - v_t\right) - E_{fd}\right] \quad (8)$$

where,

K_a and T_a = The gain and time constant of the excitation system, respectively
V_{ref} = The reference voltage

Nonlinear dynamic model of STATCOM device: As shown in Fig. 1, the STATCOM was connected at the midpoint of the transmission line, which consists of a Step Down Transformer (SDT) with leakage reactance (x_{SDT}), a three-phase Gate Turn Off (GTO) based Voltage Source Converter (VSC) and a DC capacitor.

There are two basic controllers implemented in STATCOM, i.e., a DC voltage regulator and an AC voltage regulator, as shown in Fig. 2 and 3, respectively. The VSC generates a controllable AC voltage source $v_S(t) = V_S \sin(\omega t - \psi)$ behind the leakage reactance. The difference between the STATCOM-bus AC voltage $v_s(t)$ and the power system-bus $v_m(t)$ produces the exchange of active and reactive power between the STATCOM and the power system, which can be controlled by adjusting the magnitude of V_S and the phase ψ (Bamasak and Abido, 2004):

$$v_s = cv_{DC}(\cos\psi + j\sin\psi) = cV_{DC}\angle\psi \quad (9)$$

$$c = mk \quad (10)$$

where,

m = The modulation ratio defined by Pulse Width Modulation (PWM)
k = The ratio of AC voltage to DC voltage depending on the structure of the converter
v_{DC} = The DC voltage
ψ = The phase defined by PWM

The dynamics of the capacitor voltage has a significant influence on the power system, so this must be consider. If the converter is assumed to be lossless, the active power exchanged between the converter and the system is equal to the active power that is exchanged between the capacitor and converter ($P_{DC} = P_{AC}$). So, with these assumptions, the relationship between the

voltage and current of the capacitor can be expressed as (Abido, 2005):

$$v_{DC}i_{DC} = Real(v_s i_s^*) = Real[cv_{DC}(\cos\psi + jsin\psi isd - isq] \quad (11)$$

Solving Eq. (9) for i_{DC} gives:

$$i_{DC} = c\left(i_{sd}\cos\psi + i_{sq}\sin\psi\right). \quad (12)$$

Considering Eq. (10) and the relationship between the voltage and current of the capacitor, we have:

$$\dot{v}_{DC} = \frac{c}{C_{DC}}\left(i_{sd}\cos\psi + i_{sq}\sin\psi\right). \quad (13)$$

Linearized equations of the modified Phillips-Heffron model: The linearized dynamic model of the power system equipped with the STATCOM is obtained by linearizing the nonlinear Eq. (1) to (13) around nominal operating point. The linearized model of the power system as shown in Fig. 1 is given as follows:

$$\Delta\dot{\delta} = \omega_b\Delta\omega \quad (14)$$

$$\Delta\dot{\omega} = (\Delta P_m - \Delta P_e - D\Delta\omega)/M \quad (15)$$

$$\Delta\dot{E}_q^{'} = \left[-\Delta E_q^{'} + \Delta E_{fd} - (x_d - \dot{x_d})\Delta i_d\right]/T_{do}^{'} \quad (16)$$

$$\Delta\dot{E}_{fd} = \left(-K_a\Delta v_t - \Delta E_{fd}\right)/T_a \quad (17)$$

where,

$$\Delta P_e = K_1\Delta\delta + K_2\Delta E_q^{'} + K_{pdc}\Delta V_{DC} + K_{p\psi}\Delta\psi + K_{pc}\Delta C \quad (18)$$

$$\Delta E_q^{'} = K_4\Delta\delta + K_3\Delta E_q^{'} + K_{qdc}\Delta V_{DC} + K_{q\psi}\Delta\psi + K_{qc}\Delta C \quad (19)$$

$$\Delta V_t = K_5\Delta\delta + K_6\Delta E_q^{'} + K_{vdc}\Delta V_{DC} + K_{v\psi}\Delta\psi + K_{vc}\Delta C \quad (20)$$

$$\Delta\dot{V}_{DC} = K_7\Delta\delta + K_8\Delta E_q^{'} + K_9\Delta V_{DC} + K_{dc\psi}\Delta\psi + K_{dcc}\Delta C \quad (21)$$

where, the linearization constants K_1-K_9, K_{pdc}, $K_{p\psi}$, K_{pc}, K_{qdc}, $K_{q\psi}$, K_{qc}, K_{vdc}, $K_{v\psi}$, K_{vc}, $K_{dc\psi}$ and K_{dcc} are functions of the system parameters and the initial operating conditions.

Referring to Fig. 2, the STACOM dynamic model of DC voltage regulator is described by the following state equations:

$$\Delta\dot{X}_{DC} = -K_{IDC}\Delta V_{DC} + K_{IDC}\Delta U_\psi \quad (22)$$

$$\Delta X_1 = -K_{PDC}\Delta V_{DC} + K_{PDC}\Delta U_\psi \quad (23)$$

$$\Delta X_2 = \Delta X_{DC} + \Delta X_1 \quad (24)$$

$$\Delta\dot{\psi} = \frac{K_S}{T_S}\Delta X_2 + \frac{1}{T_S}\Delta\psi \quad (25)$$

Now, substituting Eq. (24) into Eq. (25) gives:

$$\Delta\dot{\psi} = -\frac{K_{PDC}K_S}{T_S}\Delta V_{DC} - \frac{1}{T_S}\Delta\psi + \frac{K_S}{T_S}\Delta X_{DC} + \frac{K_{PDC}K_S}{T_S}\Delta U_\psi \quad (26)$$

where, K_{PDC}, K_{IDC} and ΔU_ψ are the proportional gain, integral gain and the control signal of STATCOM DC voltage regulator, respectively; K_S and T_S are the gain and time constant of the main control loop for STATCOM-ψ, respectively.

Also, from Fig. 3 the STATCOM dynamic model of AC voltage regulator is described by the following state equations:

$$\Delta\dot{X}_{AC} = -K_{IAC}f_1\Delta\delta - K_{IAC}f_2\Delta E_q^{'} - K_{IAC}f_5\Delta V_{DC} - K_{IAC}f_3\Delta\psi - K_{IAC}f_4\Delta C + K_{IAC}\Delta U_C \quad (27)$$

$$\Delta\dot{C} = -\frac{K_{PAC}K_F f_1}{T_F}\Delta\delta - \frac{K_{PAC}K_F f_2}{T_F}\Delta E_q^{'} + \frac{K_{PAC}K_F f_5}{T_F}\Delta V_{DC} - \frac{K_{PAC}K_F f_3}{T_F}\Delta\psi + \frac{K_F}{T_F}\Delta X_{AC} - \left(\frac{1}{T_F} + \frac{K_{PAC}K_F f_4}{T_F}\right)\Delta C + \frac{K_{PAC}K_F}{T_F}\Delta U_C \quad (28)$$

where,

K_F and T_F : The gain and time constant of the main control loop for STATCOM-C

$(f_1 - f_5)$: The functions of the system parameters and the initial operating conditions

K_{PAC}, K_{IAC} and ΔU_C : The proportional gain, integral gain and the control signal of STATCOM AC voltage regulator

Equation (14) to (16) and (17) describe the models for the machine and the exciter. Eq. (21), (22), (26) to (28) represent the control action of the main control loops PI/DC and PI/AC voltage regulators of the STATCOM with damping controller. In state-space representation, these equations can be arranged in compact form as:

$$\Delta\dot{X} = A\Delta X + B\Delta U, \quad (29)$$

where, the state vector ΔX, control vector ΔU, matrix A and matrix B are:

$$\Delta X = \left[\Delta\delta \;\; \Delta\omega \;\; \Delta E_q^{'} \;\; \Delta E_{fd} \;\; \Delta V_{DC} \;\; \Delta X_{DC} \;\; \Delta\psi \;\; \Delta X_{AC} \;\; \Delta C\right]^{\mathrm{T}},$$
$$\Delta U = [\Delta U_{PSS} \quad \Delta U_\psi \quad \Delta U_C]^{\mathrm{T}}$$

$$A = \begin{bmatrix} 0 & \omega_b & 0 & 0 & 0 & 0 & 0 & 0 & 0 \\ -\frac{K_1}{M} & -\frac{D}{M} & -\frac{K_2}{M} & 0 & -\frac{K_{pdc}}{M} & 0 & -\frac{K_{p\psi}}{M} & 0 & -\frac{K_{pc}}{M} \\ -\frac{K_4}{T'_{do}} & 0 & -\frac{K_3}{T'_{do}} & \frac{1}{T'_{do}} & -\frac{K_{qdc}}{T'_{do}} & 0 & -\frac{K_{q\psi}}{T'_{do}} & 0 & -\frac{K_{qc}}{T'_{do}} \\ -\frac{K_5 K_a}{T_a} & 0 & -\frac{K_6 K_a}{T_a} & -\frac{1}{T_a} & -\frac{K_{vdc} K_a}{T_a} & 0 & -\frac{K_{v\psi} K_a}{T_a} & 0 & -\frac{K_{vc} K_a}{T_a} \\ K_7 & 0 & K_8 & 0 & K_9 & 0 & K_{dc\psi} & 0 & K_{dcc} \\ 0 & 0 & 0 & 0 & -K_{IDC} & 0 & 0 & 0 & 0 \\ 0 & 0 & 0 & 0 & \frac{-K_S K_{PDC}}{T_S} & \frac{K_S}{T_S} & -\frac{1}{T_S} & 0 & 0 \\ -K_{IAC} f_1 & 0 & -K_{IAC} f_2 & 0 & -K_{IAC} f_5 & 0 & -K_{IAC} f_3 & 0 & -K_{IAC} f_4 \\ \frac{-K_F K_{PAC} f_1}{T_F} & 0 & \frac{-K_F K_{PAC} f_2}{T_F} & 0 & \frac{-K_F K_{PAC} f_5}{T_F} & 0 & \frac{-K_F K_{PAC} f_3}{T_F} & \frac{K_F}{T_F} & -\left(\frac{1}{T_F} + \frac{K_F K_{PAC} f_4}{T_F}\right) \end{bmatrix}$$

$$B = \begin{bmatrix} 0 & 0 & 0 & \frac{K_a}{T_a} & 0 & 0 & 0 & 0 & 0 \\ 0 & 0 & 0 & 0 & 0 & K_{IDC} & \frac{K_F K_{PDC}}{T_F} & 0 & 0 \\ 0 & 0 & 0 & 0 & 0 & 0 & 0 & K_{IAC} & \frac{K_F K_{PAC}}{T_F} \end{bmatrix}^T$$

System eigenvalue analysis without stabilizer: For nominal operating condition, the dynamic behavior of the system is recognized through the eigenvalues of the system matrix A. By solving the system characteristic equation $|\lambda I - A| = 0$, the eigenvalues of the system are computed which are given below:

$$\lambda_1 = -23.973, \lambda_2 - 20.051,\ \lambda_3 = -14.723, \lambda_4 = -5.358$$

$$\lambda_{5,6} = 0.375 \pm 2.282\text{i}, \lambda_7 = -20, \lambda_{8,9} = 0.486 \pm 0.367\text{i}$$

It is clearly seen from eigenvalues of the matrix A that the system is unstable and needs a supplementary stabilizer for stability.

Structure of PSS and STATCOM-POD controller: In order to overcome the LFO problem, supplemental control action must be applied to STATCOM device in form of an auxiliary damping controller, which is overlaid on the main control loops and which is called Power Oscillation Damping (POD) controller. This is illustrated in both Fig. 2 and 3.

The POD controller has a structure that is similar to that of the PSS controller. Figure 4 shows a sample block diagram of a POD controller. The controller contains three main blocks, i.e., the gain block, the washout filter block and (lead-lag) phase compensators. The washout filter block acts as a high-pass filter to eliminate the DC offset of the POD output and to prevent steady-state changes in the terminal voltage of the generator.

From this perspective, the washout time Tω should have a value in the range of 1 to 20 sec defined to the electromechanical oscillation modes and two blocks (lead-lag) phase compensators (Kundur, 1994).

In this study, the time constants, Tω, T_2 and T_4, were assigned specific values of 10s, 0.1s and 0.1s, respectively, while the parameters of the controller, i.e., K_N, T_1 and T_3 had to be determined.

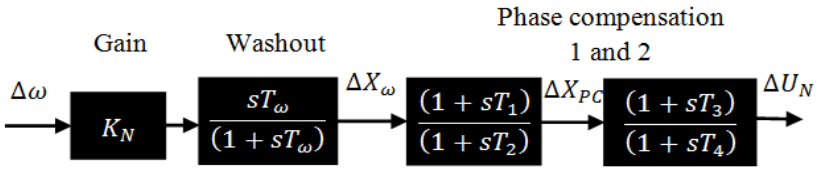

Fig. 4: Basic structure used the POD and PSS

From Fig. 4, Δω is the generator speed deviation used as an input signal to the POD and U_N is the controllers output, which was applied to any one of two STATCOM main control loops in the form of a POD or to the excitation system in the form of a PSS. By using one of the dynamic damping controllers mentioned above, the number of matrix state variables increases from 9 to 12, due to the addition of the three state variables, $\Delta\dot{X}_\omega$, $\Delta\dot{X}_{PC}$ and $\Delta\dot{U}_N$, where $N = PSS, \psi, C$.

Optimal design of the PSS or STATCOM-POD controller: The POD controller is a lead-lag type that can be described mathematically as:

$$U(s) = G(s)Y(s) \tag{30}$$

where,
$G(s)$ = The transfer function of the POD controller
$Y(s)$ = The measurement signal
$U(s)$ = The output signal from the POD controller

Which will provide additional damping by moving closed loop system modes to the left line of s-plain. Eq. (30) can be expressed in state-space form as:

$$\Delta\dot{X}_C = A_C\Delta X_C + B_C\Delta U \tag{31}$$

where, ΔX_C is the controller state vector. Equation (29) describes a linear model of the power system extracted around a certain operating point. Combining Eq. (29) with Eq. (31), we obtained a closed-loop system:

$$\Delta\dot{X}_{C\ell} = A_{c\ell}\Delta X_{C\ell} \tag{32}$$

$$\Delta X_{C\ell} = \begin{bmatrix}\Delta X \\ \Delta X_C\end{bmatrix} \tag{33}$$

$$\zeta_i = -Real(\lambda_i)/|\lambda_i| \tag{34}$$

$$J = min(\zeta_i) \tag{35}$$

where,
$\Delta X_{C\ell}$ = The state vector of the closed loop system
λ_i = The i-th eigenvalue mode of the closed loop matrix $A_{c\ell}$
ζ_i = The damping coefficient of the i-th eigenvalue

It is clear that the objective function J will identify the minimum value of the damping coefficient among modes.

The goal of the optimization process was to maximize J in order to achieve appropriate damping for all modes, including the eigenvalue of the electromechanical mode, by moving the dominant poles to the optimal location, which enhances the system's damping characteristics.

Finally, the coordinated closed loop matrix will become [15×15] in the dual-coordinated design case and [18×18] for the triple-coordinated design. The eigenvalue-based objective function J is searched for in the typical ranges of control parameters:

$$K_N^{min} \le K_N \le K_N^{max}$$

$$T_{Ni}^{min} \le T_{Ni} \le T_{Ni}^{max}$$

where, $N = PSS, \psi, C$ and $i = 1, 3$.

Typical ranges of the optimized parameters are 0.01-100 for K_N and 0.001-1 for T_{Ni}.

Optimization technique: The problem of tuning the parameters for individual and coordinated design for multiple damping controllers, which would ensure maximum damping performance, was solved via a PSO optimization procedure that appeared to be a promising evolutionary technique for handling optimization problems. PSO is a population-based, stochastic-optimization technique that was inspired by the social behavior of flocks of birds and schools of fish (Kennedy and Eberhart, 1995).

The advantages of PSO algorithm are that it is simple, easy to implement, it has a flexible and well-balanced mechanism to enhance the local and global exploration capabilities. Recently, it has acquired wide range of applications in solving optimization design problems featuring non-linearity, non-differentiability and high-dimensionality in many area search spaces (Parpinelli and Lopes, 2011).

Classical PSO algorithm: In the PSO, each possible solution is represented as a particle and each set of particles comprises a population. Each particle keeps its position in hyperspace, which is related to the fittest

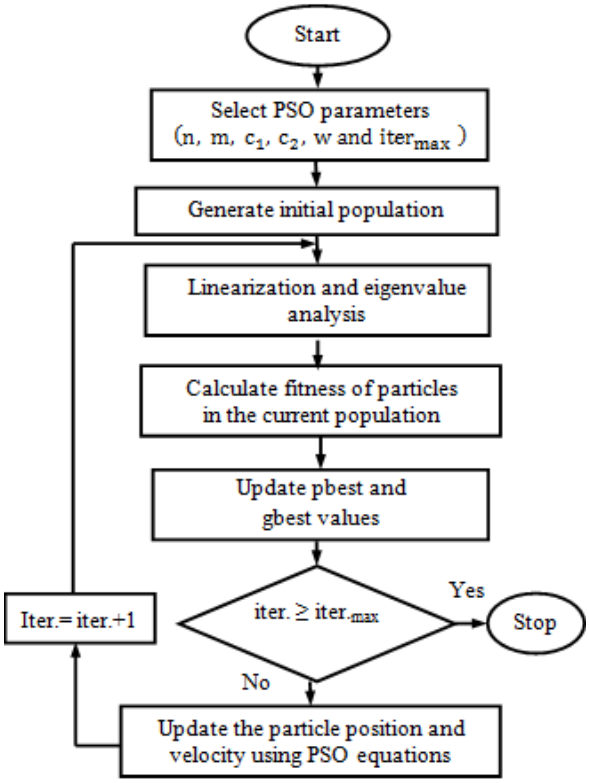

Fig. 5: PSO algorithm for the tuning parameters of an individual and coordinated design

solution it ever experiences in a special memory called $pbest$. In addition, the position related to the best value obtained so far by any particle in the population is called $gbest$. For each iteration of the PSO algorithm, the $pbest$ and $gbest$ values are updated and each particle changes its velocity toward them randomly. This concept can be expressed as (Babaei and Hosseinnezhad, 2010):

$$v_i^{k+1} = wv_i^k + c_1 r_1 (pbest_i - x_i^k) + c_2 r_2 (gbest - x_i^k) \quad (36)$$

$$x_i^{k+1} = x_i^k + v_i^{k+1}, i = 1,2,\ldots,n \quad (37)$$

where,

v = The particle velocity
x = The particle position
k = The number of iterations
w = The inertia weight factor
c_1, c_2 = The cognitive and asocial acceleration factors, respectively
n = The number of particles
r_1, r_2 = The uniformly-distributed random numbers in the range of 0 to 1

Figure 5 shows the flow chart of the PSO algorithm.

Chaotic Particle Swarm Optimization (CPSO): The main disadvantage of the simple PSO algorithm is that the performance of it greatly depends on its parameters and it is not guaranteed to be global convergent. In order to improve the global searching ability and premature convergence to local minima, PSO and chaotic sequence techniques are combined to form a Chaotic Particle Swarm Optimization (CPSO) technique, which practically combines the population-based evolutionary searching ability of PSO and chaotic searching behavior. The Logistic equation employed for constructing hybrid PSO described as (Eslami *et al*., 2011):

$$\beta^{k+1} = \mu\beta^k(1-\beta^k), 0 \le \beta^1 \le 1 \quad (38)$$

where, μ is the control parameter with a real value between 0 to 4. Although the (38) is deterministic, it exhibits chaotic dynamics when $\mu = 4$ and $\beta^0 \notin \{0, 0.25, 0.5, 0.75, 1\}$. It exhibits the sensitive dependence on initial conditions, which is the basic characteristic of chaos. The inertia weighting function in (36) is usually evaluated utilizing the following equation:

$$w = w_{max} - [(w_{max} - w_{min})(iter/iter_{max})] \quad (39)$$

where,

w_{max}, w_{min} = Maximum and minimum values of w
$iter_{max}$ = The maximum number of iterations
$iter$ = The current iteration number

The new weight parameter w_{new} is defined by multiplying weight parameter w in (39) and logistic Eq. (38):

$$w_{new} = w \times \beta^{k+1} \quad (40)$$

To improve the global searching capability of PSO, we have to introduce a new velocity update equation as follows:

$$v_i^{k+1} = w_{new} v_i^k + c_1 r_1 (\text{pbest}_i - x_i^k) + c_2 r_2 (g\text{best} - x_i^k) \quad (41)$$

We have observed that the proposed new weight decreases and oscillates simultaneously for total iteration, whereas the conventional weight decreases monotonously from w_{max} to w_{min}. The final choice of a parameter was considered to be the optimal choice: n, $iter_{max}$, c_1, c_2, w_{min}, w_{max}, μ and β^0 are chosen as 30, 100, 2, 2, 0.3, 0.9, 4 and 0.3, respectively.

RESULTS AND DISCUSSION

In this section, the abilities of the proposed dual and triple coordinated designs are investigated in order

Table 1: Power system load conditions

Load condition	P (P. U.)	Q (P. U.)
Nominal	1	0.20
Heavy	1.2	0.25

to damp the LFO and improve the dynamic stability of the power system.

To evaluate the performance of the proposed simultaneous coordinated designs, the responses with the proposed controllers were compared with the responses of the individual design controllers, PSS and STATCOM.

To support the result of the eigenvalue analysis, the performances of the system with dual and triple coordinated controllers were tested with a 10% step change in the input mechanical power for two different loading conditions are given in Table 1.

The resultant optimal parameters of the individual controllers, dual and triple coordinated designs are given in Table 2 to 4, respectively.

Figure 6 to 9 show the system responses of speed deviation with 10% step change in mechanical input power where the dual-coordinated design control

Table 2: The optimal parameters of the individual controllers at nominal and heavy conditions

		Optimal values		
Individual controllers	Type of condition	K	T_1 (Sec)	T_3 (Sec)
PSS	Nominal	7.0168	0.9641	0.7223
	Heavy	11.6804	0.6373	0.1157
ψ	Nominal	60.0180	0.5971	0.3638
	Heavy	49.7432	0.9523	0.0051
C	Nominal	0.2138	0.0637	0.3547
	Heavy	3.0016	0.4006	0.0081

Table 3: The optimal parameters of the different dual-coordinated designs at nominal and heavy conditions

		Optimal values					
Coordinated designs	Type of condition	K^*	T_1^* (Sec)	T_3^* (Sec)	$K^\#$	$T_1^\#$ (Sec)	$T_3^\#$ (Sec)
PSS*&$\psi^\#$	Nominal	50.4080	0.1671	0.1589	99.8780	0.2645	0.16930
	Heavy	52.7647	0.1553	0.1547	99.8817	0.3736	0.47840
PSS*&C$^\#$	Nominal	14.2617	0.9931	0.8356	2.5712	0.8593	0.92540
	Heavy	16.2846	0.7912	0.5718	3.8110	0.9759	0.75150
ψ^*&C$^\#$	Nominal	99.9997	0.6683	0.0681	1.4761	1	0.79540
	Heavy	100	0.4977	0.1888	2.3317	0.9026	0.86367

Table 4: The optimal parameters of the triple-coordinated design at nominal and heavy conditions

		Optimal values								
Coordinated designs	Type of condition	K^{PSS}	T_1^{PSS} (Sec)	T_3^{PSS} (Sec)	K^ψ	T_1^ψ (Sec)	T_3^ψ (Sec)	K^C	T_1^C (Sec)	T_3^C (Sec)
PSS &ψ& C	Nominal	58.5828	0.1632	0.0268	79.5733	0.3311	0.0504	1.0438	0.0364	0.8879
	Heavy	64.5110	0.0338	0.2282	65.5158	0.3748	0.6972	0.0811	0.1233	0.3170

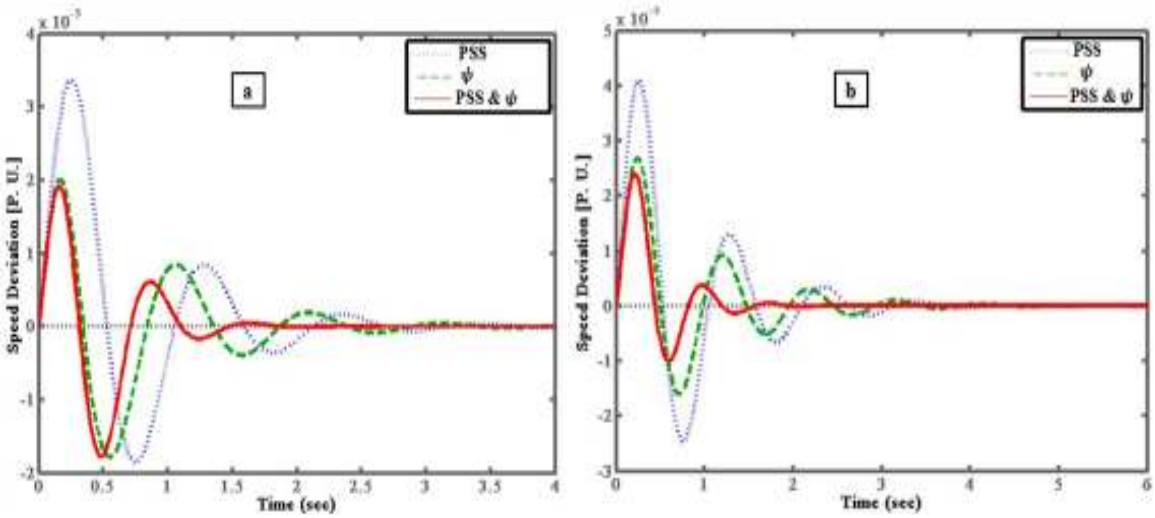

Fig. 6: Dynamic responses for Δω with different damping controllers (individual PSS, ψ and dual coordinated design PSS &ψ), a) nominal load, b) heavy load

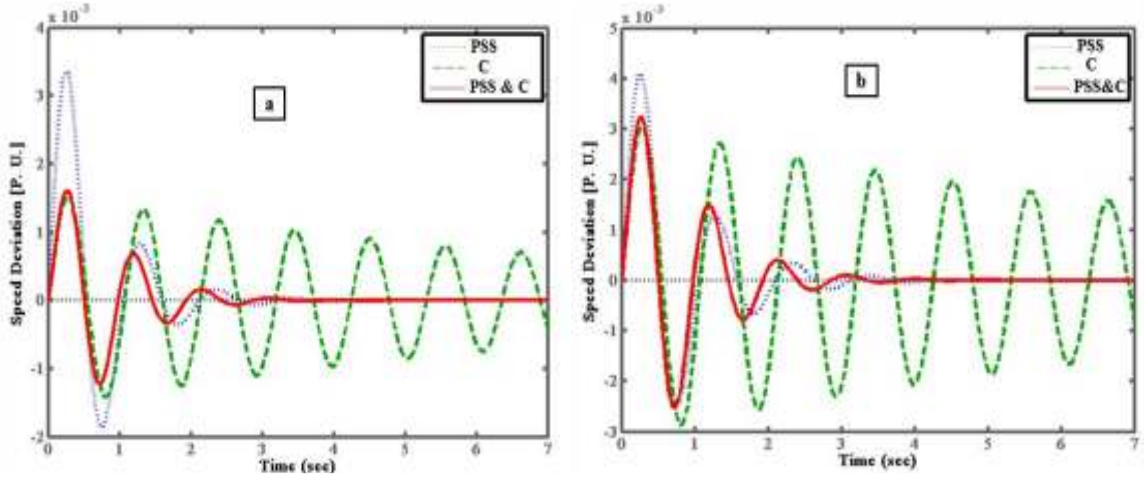

Fig. 7: Dynamic responses for Δω with different damping controllers (individual PSS, C and dual coordinated design PSS & C) at, a) nominal load, b) heavy load

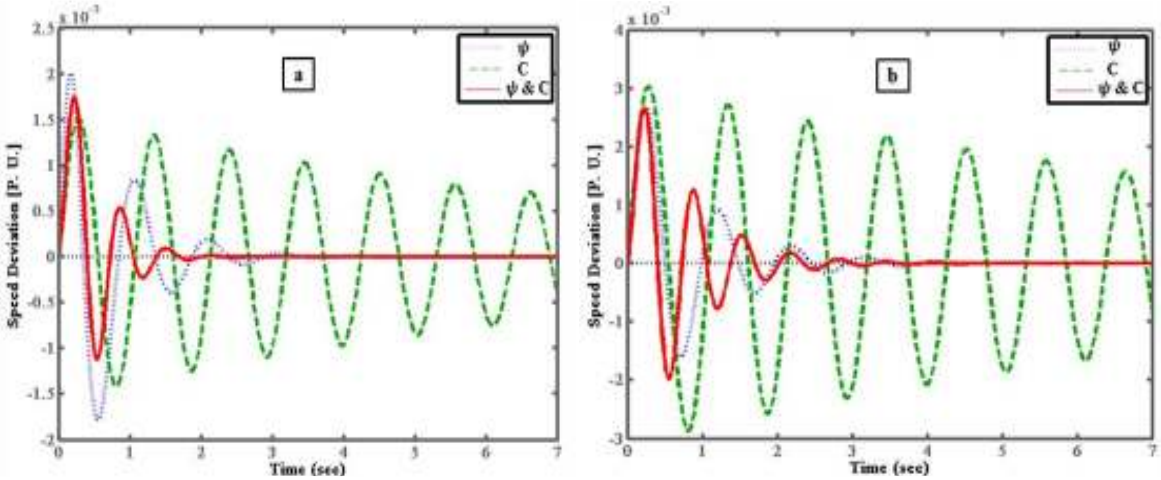

Fig. 8: Dynamic responses for Δω with different damping controllers (individualψ, C and dual coordinated design ψ& C) at, a) nominal load, b) heavy load

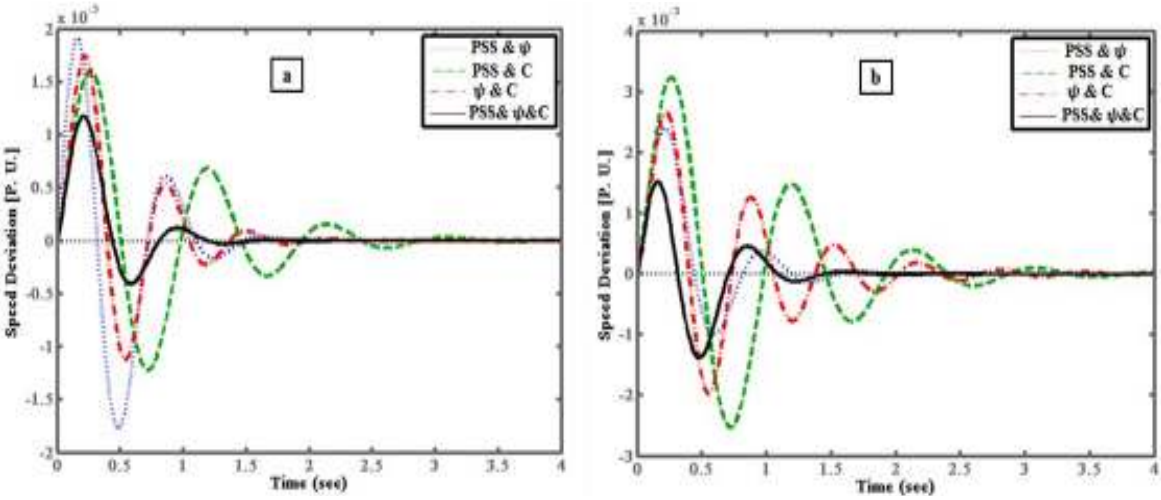

Fig. 9: Dynamic responses for Δω with different damping controllers (dual and triple coordinated design) at, a) nominal load, b) heavy load

Table 5: System eigenvalues of the individual designs at nominal and heavy conditions

PSS		ψ		C	
Nominal	Heavy	Nominal	Heavy	Nominal	Heavy
$-1.12 \pm j4.43$	$-0.96 \pm j4.43$	$-2.88 \pm j6.72$	$-1.71 \pm j4.64$	$-0.27 \pm$ j4.62	$-0.35 \pm$ j7.5
$\zeta_{EM} = 0.2451$	$\zeta_{EM} = 0.2118$	$\zeta_{EM} = 0.3939$	$\zeta_{EM} = 0.3458$	$\zeta_{EM} = 0.0583$	$\zeta_{EM} = 0.0466$
$-18.58 \pm j4.37$	$-1.15 \pm j4.68$	$-9.91 \pm$ j7.09	$-2.36 \pm$ j3.71	-19.742	-14.80
-19.61	$-2.52 \pm j5.20$	$-1.47 \pm$ j5.11	$-3.05 \pm$ j6.69	-18.822	$-0.06 \pm j3.47$
$-4.84 \pm j7.01$	-15.93	-29.31	$-3.17 \pm$ j1.23	$-10.25 \pm j5.81$	-5.29
$-1.55 \pm j3.85$	$-11.78 \pm j6.37$	$-2.26 \pm$ j3,36	-19.48	$-0.72 \pm j2.94$	-0.82
-12.46	$-4.10 \pm j4.88$	-14.67	$-15.68 \pm j7.93$	-10.02	$-0.98 \pm j4.05$
-0.25	-0.24	-1.69	-5.73	-9.11	-2.68
-0.20		-1.35		-0.24	-0.13
				-0.20	-0.29

Table 6: System eigenvalues of the dual-coordinated designs at nominal and heavy conditions

PSS & ψ		PSS & C		ψ & C	
Nominal	Heavy	Nominal	Heavy	Nominal	Heavy
$-4.56 \pm j7.25$	$-2.34 \pm j4.09$	$-2.93 \pm j5.76$	$-1.45 \pm j3.20$	$-3.91 \pm$ j6.41	$-1.65 \pm j3.36$
$\zeta_{EM} = 0.5324$	$\zeta_{EM} = 0.4966$	$\zeta_{EM} = 0.4534$	$\zeta_{EM} = 0.4127$	$\zeta_{EM} = 0.5207$	$\zeta_{EM} = 0.4408$
$-4.22 \pm j8.18$	$-3.25 \pm j3.09$	$-20.4 \pm j1.98$	$-9.86 \pm j5.04$	$-10.18 \pm j7.31$	$-2.51 \pm j4.26$
-7.63	$-10.36 \pm j2.69$	$-2.18 \pm j3.63$	$-6.11 \pm j6.89$	$-7.68 \pm j9.80$	$-8.10 \pm j6.13$
$-4.37 \pm j5.78$	-8.23	$-4.11 \pm j6.58$	-4.56	-35.14	$-13.04 \pm j7.58$
$-6.26 \pm j9.48$	-0.73	-10.05	$-2.35 \pm j3.77$	-9.23	-19.66
$-5.31 \pm j5.85$	$-12.56 \pm j5.78$	$-3.24 \pm j4.86$	-8.76	$-8.55 \pm$ j9.87	-5.91
-1.21	$-5.4 \pm j6.27$	$-2.08 \pm j3.58$	-3.28	-28.75	$-9.17 \pm j2.62$
-27.76	-17.02	-21.6	$-8.47 \pm j5.90$	-4.07	$-2.42 \pm j3.08$
-23.13	-11.93	-0.25	-13.21	-0.84	-0.27
-0.25	-0.18		-0.20	-6.64	
				-0.20	

Table 7: System eigenvalues of the triple-coordinated design at nominal and heavy conditions

PSS & ψ & C	
Nominal	Heavy
$-3.74 \pm j4.05$	$-2.96 \pm j3.85$
$\zeta_{EM} = 0.6784$	$\zeta_{EM} = 0.6095$
$-3.59 \pm j3.52$	$-4.26 \pm j4.50$
$-4.09 \pm j3.39$	$-7.27 \pm j8.31$
-27.97	-11.20
-6.53	$-3.74 \pm$ j4.65
$-13.84 \pm j8.12$	$-17.33 \pm j9.14$
$-5.85 \pm j1.14$	-12.37
-10	-9.83
-15.37	$-11.48 \pm j7.66$
$-2.69 \pm$ j2.87	-18.90
-1.38	-0.83
-0.20	-0.20

between (PSS & STATCOM ψ-based POD, PSS & STATCOM *C*-based POD and STATCOM ψ-based POD and STATCOM *C*-based POD) was compared to their individual stabilizers. The system eigenvalues with the proposed individual stabilizers and coordinated designs for nominal and heavy operating conditions are given in Table 5 and 6, respectively. The first and second rows represent the electromechanical mode and their damping ratio ζ_{EM} using participation factor to identify the eigenvalue associated with electromechanical mode. It is clear that the dual-coordinated design control greatly improved the system damping compared with individual controllers and the coordinated design control solved the problem of low damping when only the STATCOM *C*-based POD was considered.

Figure 9 shows the system responses of speed deviation with 10% step change in mechanical input power where the triple-coordinated design control among (PSS & STATCOM ψ-based POD & STATCOM *C*-based POD) was compared to different dual-coordinated designs, all on one figure for better clarification. It can be seen from the results that the better dynamic response was obtained by triple-coordinated design control, which was much faster and had, less setting time and overshoot than the individual and dual-damping controllers. The eigenvalues of the system with the triple-coordinated design are given in Table 7.

CONCLUSION

In this study, we focused on damping of low-frequency oscillations via PSS and STATCOM-based POD applied independently and also through the simultaneous dual-and triple-coordinated designs of the multiple damping controllers in a SMIB power system. For the proposed damping controller design problem, a CPSO algorithm was used as the optimization technique to search for the optimal damping controller parameters in both the individual and the coordinated designs. The simulation results showed the superiority of the dual-coordinated design over the individual design because it improved the system's damping characteristics at different loading conditions. In addition, the dual-coordinated design solved the problem of low-effect damping when the STATCOM

C-based POD was applied to the system. The triple-coordinated design provided better dynamic response than the individual and the dual-coordinated design control at nominal and heavy loading conditions.

APPENDIX

Power system parameters (resistance and reactance are in p.u. and time constants are in second):

Generator: $M = 6$, $T'_{do} = 7.76$, $x_q = 0.55$, $x_d = 1$, $\dot{x_d} = 0.3$ and D = 4

Excitation: $K_a = 50$, $T_a = 0.05$

Transmission line: $R = 0, x_1 = 0.3, x_2 = 0.3$

STATCOM: $\psi_o = 46.25^o, c_o = 0.25, C_{DC} = 1, V_{DC} = 1, K_S = K_F = 1, T_S = T_F = 0.5, x_{SDT} = 0.15$
$K_{IDC} = K_{IAC} = 0.2$, $K_{PDC} = K_{PAC} = 0$.

REFERENCES

Abd-Elazim, S.M. and E.S. Ali, 2012. Coordinated design of PSSs and SVC via bacteria foraging optimization algorithm in a multimachine power system. Int. J. Elec. Power, 41(1): 44-53.

Abdel-Magid, Y.L. and M.A. Abido, 2004. Robust coordinated design of excitation and TCSC-based stabilizers using genetic algorithms. Electr. Pow. Syst. Res., 69(2-3): 129-141.

Abido, M.A., 2005. Analysis and assessment of STATCOM-based damping stabilizers. Electr. Pow. Syst. Res., 73(1): 177-185.

Babaei, E. and V. Hosseinnezhad, 2010. A QPSO based parameters tuning of the conventional power system stabilizer. Proceedings of 9th International Power and Energy Conference (IPEC, 2010), pp: 467-471.

Babaei, E., A.M. Bolhasan, M. Sadeghi and S. Khani, 2011. An improved PSO and genetic algorithm based damping controller used in UPFC for power system oscillations damping. Proceedings of the International Conference on Electrical Machines and Systems (ICEMS 2011), pp: 1-6.

Bamasak, S.M. and M.A. Abido, 2004. Assessment study of shunt FACTS-based controller's effectiveness on power system stability enhancement. Proceedings of the 39th International Universities Power Engineering Conference (UPEC 2004). Saudi Electricity Co., pp: 274-278.

Du, W., X. Wu, H.F. Wang and R. Dunn, 2010. Feasibility study to damp power system multi-mode oscillations by using a single FACTS device. Int. J. Elec. Power, 32(6): 645-655.

Eslami, M., H. Shareef, A. Mohamed and M. Khajehzadeh, 2011. Coordinated design of PSS and SVC damping controller using CPSO. Proceedings of the 5th International Power Engineering and Optimization Conference 2011 (PEOCO 2011), pp: 11-16.

Furini, M.A., A.L.S. Pereira and P.B. Araujo, 2011. Pole placement by coordinated tuning of power system stabilizers and FACTS-POD stabilizers. Int. J. Elec. Power, 33(3): 615-622.

Gibbard, M.J., D.J. Vowles and P. Pourbeik, 2000. Interactions between and effectiveness of, power system stabilizers and FACTS device stabilizers in multimachine systems. IEEE T. Power Syst., 15(2): 748-755.

Hemmati, R., S.M.S. Boroujeni, E. Behzadipour and H. Delafkar, 2011. Supplementary stabilizer design based on STATCOM. Indian J. Sci. Technol., 4(5): 525-529.

Kazemi, A. and V.M. Sohrforouzani, 2006. Power system damping using fuzzy controlled facts devices. Int. J. Elec. Power, 28(5): 349-357.

Kennedy, J. and R.C. Eberhart, 1995. Particle swarm optimization. Proceedings of the IEEE International Conference on Neural Networks. Perth, pp: 1942-1948.

Kundur, P., 1994. Small-signal Stability. In: Balu, N.J. and M.G. Lauby (Eds.), Power System Stability and Controls. McGraw-Hill, Inc., New York, pp: 699-717.

Li, S.Y., S.S. Lee, Y.T. Yoon and J.K. Park, 2009. Nonlinear adaptive decentralized stabilization control for multimachine power systems. Int. J. Control Autom., 7(3): 389-397.

Mohagheghi, S., G.K. Venayagamoorthy and R.G. Harley, 2007. Optimal neuro-fuzzy external controller for a STATCOM in the 12-bus benchmark power system. IEEE T. Power Deliver., 22(4): 2548-2558.

Mostafa, H.E., M.A. El-Sharkawy, A.A. Emary and K. Yassin, 2012. Design and allocation of power system stabilizers using the particle swarm optimization technique for an interconnected power system. Int. J. Elec. Power, 34(1): 57-65.

Mukherjee, V. and S.P. Ghoshal, 2007. Comparison of intelligent fuzzy based AGC coordinated PID controlled and PSS controlled AVR system. Int. J. Elec. Power, 29(9): 679-689.

Nguyen, T.T. and R. Gianto, 2008. Neural networks for adaptive control coordination of PSSs and FACTS devices in multimachine power system. IET Gener. Transm. Dis., 2(3): 355-372.

Panda, S. and N.P. Padhy, 2008. Optimal location and controller design of STATCOM for power system stability improvement using PSO. J. Franklin I., 345(2): 166-181.

Parpinelli, R.S. and H.S. Lopes, 2011. New inspirations in swarm intelligence: A survey. Int. J. Bio-Inspired Comput., 3(1): 1-16.

Rouco, L., 2001. Coordinated design of multiple controllers for damping power system oscillations. Int. J. Elec. Power, 23(7): 517-530.

Segal, R., A. Sharma and M.L. Kothari, 2004. A self-tuning power system stabilizer based on artificial neural network. Int. J. Elec. Power, 26(3): 423-430.

Shayeghi, H., A. Safari and H.A. Shayanfar, 2010. PSS and TCSC damping controller coordinated design using PSO in multi-machine power system. Energ. Convers. Manage., 51(12): 2930-2937.

Talaat, H.E.A., A. Abdennour and A.A. Al-Sulaiman, 2010. Design and experimental investigation of a decentralized GA-optimized neuro-fuzzy power system stabilizer. Int. J. Elec. Power, 32(7): 751-759.

Yao, F.T.S., 1983. Electric Power System Dynamics. 1st Edn., Academic Press, Inc., New York, USA.

Zhang, X.P., C. Rehtanz and B. Pal, 2006. Flexble AC Transmission system: Modeling and Control. Springer, Berlin Heidelberg.